Computational ghost imaging of hot objects in long-wave infrared range

Zhang, Shuang; Liu, Hong-Chao

DOI:
10.1063/1.4994662

License:
Other (please specify with Rights Statement)

Document Version
Peer reviewed version

Citation for published version (Harvard):
Zhang, S & Liu, H-C 2017, 'Computational ghost imaging of hot objects in long-wave infrared range', *Applied Physics Letters*, vol. 111, 031110. https://doi.org/10.1063/1.4994662

Computational ghost imaging of hot objects in long-wave infrared range

Hong-Chao Liu[1, a)] and Shuang Zhang[1, b)]
[1] *School of Physics and Astronomy, University of Birmingham, Birmingham B15 2TT, United Kingdom*

(Dated: 4 July 2017)

Ghost imaging (GI) is an intriguing imaging modality to obtain the object information from the correlation calculations of spatial intensity fluctuations. In this Letter, we report computational GI of hot objects in the long-wave infrared range both in experiment and simulation. Without employing an independent light source, we reconstruct thermal images of objects only based on the intensity correlations of their thermal radiation at room temperature. By comparing different GI reconstruction algorithms, we demonstrate that GI with compressive sensing can efficiently obtain the thermal object information only with a single-pixel infrared camera, which might be applied to night-vision, environmental sensing, military detection, etc.

Different from the Michelson interferometer describing the first-order field correlation, intensity interferometer pioneered by Hanbury Brown and Twiss (HBT) focused on the second-order correlation of light intensity fluctuations and introduced a great method to measure the stellar sizes[1,2] and the images of hot stars in astronomy[3,4]. Beyond astrophysics, HBT experiment also sparked the studies of optical coherence theory in quantum optics[5]. Recently, a spatial HBT-type imaging modality, called ghost imaging (GI)[6–8], attracted much research attention. Similar to the principle of HBT experiment, GI obtains the object information through the correlation of light intensity fluctuations of two beams: one (i.e. object beam) that interacts with the object and is bucket detected without spatial resolution; and the other (i.e. reference beam) that does not interact with the object and is recorded by a spatially resolved multi-pixel detector. In 1995, Pittman et al. reported the first experimental realization of GI with entangled photon pairs and interpreted it as a quantum effect.[9] Later, Bennink et al. experimentally demonstrated that the GI phenomenon could also be observed with a classical light source,[10] which raised a debate whether GI has a quantum or classical nature[6,8,11] and also sparked considerable studies of GI both in theory and experiment[12–41]. Due to its robustness against the noise and turbulent atmosphere in imaging process,[18,21] GI has great potential in optical communications, optical encryption, medical imaging, and environmental sensing,[16–23] compared with traditional imaging techniques. To steer the GI technique towards the practical applications, many different GI schemes and algorithms were developed to enhance the imaging efficiency and the imaging quality, including high-order GI,[24–26] computational GI,[27] compressive GI,[28] differential GI,[29] and normalized GI,[30] etc.

Meanwhile, light sources play an important role to deepen the understanding of the GI nature and broaden the GI applications. So far, GI has been extensively studied with different bosonic sources, including the entangled light,[9,31] pseudothermal / thermal visible light,[10,11,13,14,16–23] near-infrared source,[32–35] fluorescent source,[36] X-ray,[37,38] and massive ^{4}He atom.[39] In addition, GI with chaotic fermions has also been investigated theoretically.[40,41] Apart from the various sources above, the long-wave infrared radiation source (wavelength: 8-15 μm), i.e. the thermal radiation coming from the imaging object itself, has not caught much attention for the GI technique.

In this Letter, we report the computational GI of hot objects in the long-wave infrared range both in experiment and simulation. We recover the thermal images of the object targets by measuring the spatial intensity correlations of their blackbody radiation, instead of employing any independent light sources. This external-source-free GI is similar to the HBT experiment but different from previous GI schemes, which thereby verifies the strong connection and unified physics between GI and HBT experiment[42]. Furthermore, by comparing different GI reconstruction algorithms, we demonstrate that GI with compressive sensing can efficiently obtain the thermal object information only with a single-pixel infrared camera, which has potential applications in the night-vision, military detection and environmental sensing, etc.

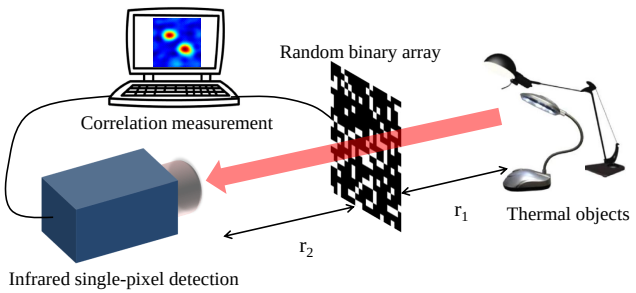

FIG. 1. Experimental setup of computational ghost imaging with thermal objects in long-wave infrared range.

Based on the classical interpretation, computational GI uses a computational intensity fluctuation pattern to

[a)] Author to whom correspondence should be addressed. Electronic mail: hongcao@connect.ust.hk
[b)] Author to whom correspondence should be addressed. Electronic mail: s.zhang@bham.ac.uk

replace the reference beam and only employs a single-pixel detector,[27] which largely simplifies the experimental setup, in comparison to the traditional two-detectors GI. It is worth mentioning that an interesting technique, called single-pixel camera, also enables single-pixel detection with a random mask or projected light patterns (usually created by spatial light modulator or digital micromirror device), which shares similar features with computational GI. Moreover, in image reconstruction process, both of them employ the same algorithms, which will be discussed later. The experimental setup of computational GI with hot objects is shown in Fig.1. The hot objects here are two table lamps and the FLUKE TiX560 infrared camera is employed as the bucket detector (or single-pixel detector). Between the thermal objects and detector, a 51×51 pixels random binary mask ($X^{m\times m}$) with the size of 145.35 mm × 145.35 mm is placed. The random binary masks are printed on regular paper sheets with a transmissive-pixel to nontransmissive-pixel ratio as 1:99. The distance from the table lamps to the mask is set as $r_1 = 250$ mm; and the distance from the mask to the detector is $r_2 = 550$ mm. In contrast to general computational GI and traditional two-detector GI scheme, no external light source, i.e. neither active nor passive illumination, is necessary in our experiment. The blackbody radiation emitting from the imaging object itself plays the role of light source. As shown in Fig. 1, the thermal radiation emitting from the imaging objects goes though the random binary mask and is detected by the infrared camera, where only the total radiation intensity Y arriving at the camera plane is recorded. According to the GI reconstruction algorithm, the thermal image can be recovered by correlation calculation between $\{X_N^{m\times m}\}$ and $\{Y_N\}$ after N times sampling measurements.

Applying different reconstruction calculation algorithms usually leads to different recovered ghost image qualities. Here, we compare three different correlation algorithms, i.e. standard GI, differential ghost imaging (DGI) and compressive ghost imaging (CGI) with our thermal radiation objects. According to the standard GI, the object information can be retrieved with the second-order spatial intensity correlation function defined as[19,27]

$$G^{(2)}(x,y) = \frac{1}{N}\sum_{i=1}^{N}\left[Y_i - \langle Y\rangle\right] X_i(x,y), \qquad (1)$$

where Y_i is the bucket signal of the object beam in the i-th measurement. $\langle\cdots\rangle$ represents the average value of N measurements. $X_i(x,y)$ is the intensity distribution of the reference beam in the $x-y$ plane, which becomes a random binary array $X_i^{m\times m}$ in the computational GI scheme. Developing from the definition in Eq.(1), the differential bucket signal in the DGI algorithm is defined as[29]

$$Y_i^{DGI} = Y_i - \frac{\langle Y\rangle}{\langle X\rangle} X_i, \qquad (2)$$

where $X_i = \int X_i(x,y)dxdy$ is the total intensity of the reference beam or the sum of the random binary array $X_i^{m\times m}$ in the i-th measurement.

Different from the standard GI and DGI algorithms, a compressive sensing algorithm was introduced into the GI technique recently,[28] based on the sparsity of the imaging object. In computational CGI, the random binary array $X_i^{m\times m}$ is reshaped into a row vector ($1\times K$, $K = m\times m$), and the set $\{X_N^{m\times m}\}$ of N measurements is rewritten as a two-dimensional matrix A ($N\times K$). Meanwhile, the set of bucket signal $\{Y_N\}$ is expressed as a column vector Y^{CGI} ($N\times 1$). Assuming the object image is sparse in matrix A, it can be reconstructed by solving the convex optimization program as[21,28]

$$T^{CGI} = |\,T\,|\,,\ \min \|\,T\,\|_1 \ \text{ subject to } \ Y^{CGI} = AT, \quad (3)$$

where T^{CGI} is the recovered image information, T is the imaging object information, and $\|\,T\,\|_1$ is the L_1-norm of T.

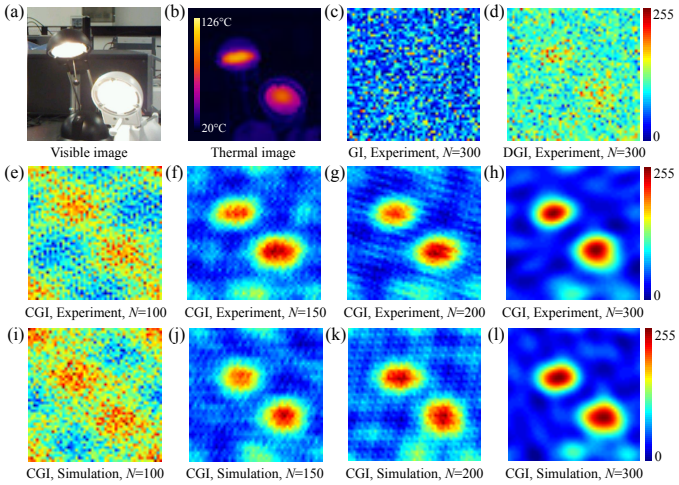

FIG. 2. Experimental object images with direct multi-pixel detection in (a) visible light range and (b) long-wave infrared range. Experimentally reconstructed images (51×51 pixels) with (c) standard GI and (d) DGI algorithms in 300 measurements. (e)-(h) Experimentally reconstructed images and (i)-(l) simulated reconstructed images with CGI algorithm. The measurement number N ranges from 100 to 300 in (e)-(l).

Figure 2 shows the experiment and simulation results with two table lamps as thermal imaging objects. Comparing with the image in the visible light range (Fig. 2(a)), the thermal radiation image (Fig. 2(b)), which is obtained from the direct multi-pixel measurement, only shows the objects with different temperature from the surrounding atmosphere. By performing 300 measurements with different random binary masks, no recognizable ghost image can be reconstructed by applying the standard GI and DGI algorithm experimentally, as shown in Figs. 2(c) and (d). Nevertheless, DGI does show some contrasts between the background and the object areas,

demonstrating its improvement from the standard GI. As shown in Figs. 2(e)-(l), CGI recovers the thermal image when $N > 150$ both in experiment and simulation, where Fig. 2(b) acts as the imaging object in the simulation. When $N = 300$, Figs. 2(h) and (l) clearly reconstruct the two bulbs areas with high temperature and even recover the two lamp holders with weak thermal radiation as well. It should be mentioned that the resolution of the reconstructed image depends on the pixels of random mask (51×51 pixels). The direct multi-pixel detection, as illustrated by Fig. 2(b), is measured through a window of the same size as the random mask, while the same experimental condition (i.e. distance from object to detector) as the corresponding bucket detection with random masks is maintained.

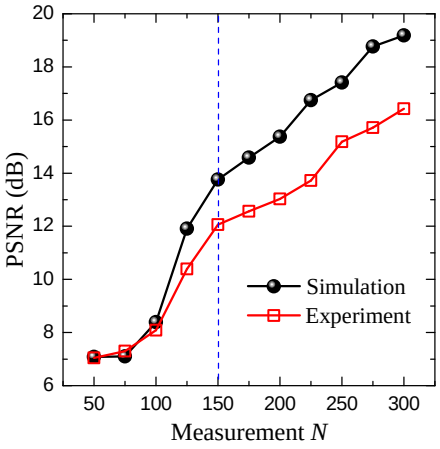

FIG. 3. Experimental and simulated PSNR value versus measurement number N for the CGI case in Fig. 2.

To quantitatively estimate the recovered image quality, we introduce the peak signal-to-noise ratio (PSNR) as

$$\mathrm{PSNR} = 10\log_{10}\left(\frac{\mathrm{MAX}^2}{\mathrm{MSE}}\right), \tag{4}$$

where MAX = 255 is the maximum possible pixel value of the image in our case. MSE is the mean square error, given by $\frac{1}{m\times m}\sum_{i,j}\left[T_{re}(x_i,y_j) - T(x_i,y_j)\right]^2$, where $T_{re}(x_i,y_j)$ and $T(x_i,y_j)$ are the pixel values of the recovered image (e.g. Figs. 2(e)-(l)) and the imaging object (e.g. Fig. 2(b)), respectively.[21,28] From Fig. 3, one can see that both experiment and simulation curves show the same variation trend. When $N < 100$, the PSNR values are around 7 and the recovered ghost images are submerged in the noise, as shown in Figs. 3, 2(e) and (i). Then, a dramatic increase of PSNR occurs when $100 < N < 150$, and a recognizable ghost image starts to appear. As N keeps increasing, both the PSNR value and the recovered image quality monotonically increase as shown in Fig. 3 and 2(e)-(l).

To further test the single-pixel computational CGI scheme with the thermal radiation in the long-wave infrared range, we choose a room-temperature figurine as an object and introduce a hot background (∼65 °C) with a hotplate, as shown in Fig. 4. Both object and background radiations are located in the long-wave infrared range (8-15 μm). Moreover, the figurine is covered by a blue plastic bag, which largely weakens the visibility in the visible and near-infrared range, as shown in Fig. 4(a). In the experiment, the distance from the figurine to the random binary mask is $r_1 = 300$ mm; and the distance from the mask to the detector is kept as $r_2 = 550$ mm. When $N = 660$, standard GI reconstruction algorithm fails to provide a ghost image (Fig. 4(c)), but the outline of reconstructed image can be roughly recognized by employing DGI, as shown in Fig. 4(d). Representing a significant advantage, CGI rebuilds the outline of thermal ghost image when $N = 300$ both in experiment and simulation, as shown in Fig. 4(f) and (j). As N further increases, one can see that more image details are reconstructed in Figs. 4(g) ,(h), (k) and (l), by viewing the Fig. 4(b) (i.e. the image from the direct multi-pixel measurement) as a reference. It is worth mentioning that fewer measurements (i.e. a smaller N) are taken to obtain a clearer thermal image for the lamps than the figurine. It is because that the lamp image is sparser than the figurine image. The sparser the image, the fewer measurements are required based on the concept of compressive sensing algorithm. Nevertheless, the measurement number to achieve a recognizable image is still much less than the Nyquist limit ($N = 51\times51 = 2601$).[21,28] By enhancing the pixel of random binary mask, as well as the measurement number, the quality of the recovered ther-

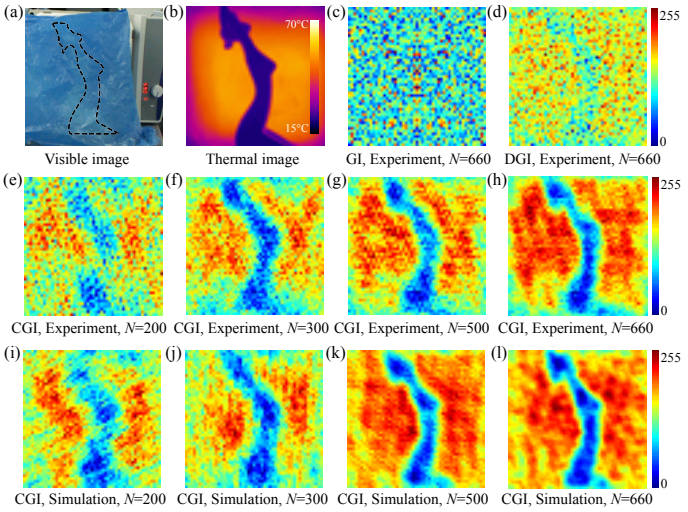

FIG. 4. Experimental object images with direct multi-pixel detection in (a) visible light range and (b) long-wave infrared range. The imaging object in (a) is covered by a blue plastic bag, and the dash curve shows the location of the object. Experimentally reconstructed images (51×51 pixels) with (c) standard GI and (d) DGI algorithms in 660 measurements. (e)-(h) Experimentally reconstructed images and (i)-(l) simulated reconstructed images with CGI algorithm. The measurement number N ranges from 200 to 660 in (e)-(l).

mal image is expected to have a further improvement.

In summary, the computational GI of hot objects in the long-wave infrared range has been studied. Without any external light source, we have reconstructed the thermal images of the targets only depending on the spatial intensity correlations of their thermal radiation. We have compared different GI reconstruction algorithms and demonstrated that GI with compressive sensing can efficiently obtain the thermal object information only with a single-pixel infrared camera, which paves the way to the simplification of the infrared camera and the applications in night-vision, environmental sensing, military intelligence gathering, etc.

We acknowledge Jinhui Shi, Qinghua Guo and Biao Yang for their helpful discussions. This work was supported by ERC Consolidator Grant (Topological).

[1]R. H. Brown and R. Q. Twiss, Nature (London) 177, 27 (1956).
[2]R. H. Brown and R. Q. Twiss, Nature (London) 178, 1046 (1956).
[3]M. Zhao, J. D. Monnier, E. Pedretti, N. Thureau, A. Mérand, T. Ten Brummelaar, H. McAlister, S. T. Ridgway, N. Turner, J. Sturmann, et al., The Astrophys. J. 701, 209-224 (2009).
[4]D. Dravins, S. LeBohec, H. Jensen, P. D. Nuñez, and CTA Consortium, Astropart. Phys. 43, 331-347 (2013).
[5]R. J. Glauber, Phys. Rev. 130, 2529 (1963).
[6]Y. H. Shih, e-print arXiv: 0805.1166 (2008).
[7]B. I. Erkmen and J. H. Shapiro, Adv. in Opt. and Photon. **2**, 405-450 (2010).
[8]J. H. Shapiro and R. W. Boyd, Quantum Inf. Processing, **11**, 949-993 (2012).
[9]T. B. Pittman, Y. H. Shih, D. V. Strekalov, and A. V. Sergienko, Phys. Rev. A, **52**, R3429(R) (1995).
[10]R. S. Bennink, S. J. Bentley, and R. W. Boyd, Phys. Rev. Lett. **89**, 113601 (2002).
[11]G. Scarcelli, V. Berardi, and Y. Shih, Phys. Rev. Lett. **96**, 063602 (2006).
[12]K. Wang and D.-Z. Cao, Phys. Rev. A **70**, 041801(R) (2004).
[13]F. Ferri, D. Magatti, A. Gatti, M. Bache, E. Brambilla, and L. A. Lugiato, Phys. Rev. Lett. **94**, 183602 (2005).
[14]A. Valencia, G. Scarcelli, M. DAngelo, and Y. Shih, Phys. Rev. Lett. **94**, 063601 (2005).
[15]Y. Cai and S.-Y. Zhu, Phys. Rev. E **71**, 056607 (2005).
[16]R. Meyers, K. S. Deacon, and Y. Shih, Phys. Rev. A **77** 041801(R) (2008).
[17]X. H. Chen, Q. Liu, K. H. Luo, and L. A. Wu, Opt. Lett. **34**, 695-697 (2009).
[18]J. Cheng, Opt. Exp. **17**, 7916-7921 (2009).
[19]P. Clemente, V. Durán, E. Tajahuerce, and J. Lancis, Opt. Lett. **35**, 2391-2393 (2010).
[20]R. E. Meyers, K. S. Deacon, and Y. Shih, Appl. Phys. Lett, **98**, 111115 (2011).
[21]C. Zhao, W. Gong, M. Chen, E. Li, H. Wang, W. Xu, S. Han, Appl. Phys. Lett. **101**, 141123 (2012).
[22]B. Sun, M. P. Edgar, R. Bowman, L. E. Vittert, S. Welsh, A. Bowman, and M. J. Padgett, Science, **340**, 844-847 (2013).
[23]P. Ryczkowski, M. Barbier, A. T. Friberg, J. M. Dudley, and G. Genty, Nat. Photon. **10**, 167-170 (2016).
[24]D. -Z. Cao, J. Xiong, S. H. Zhang, L. F. Lin, L. Gao, and K. Wang, Appl. Phys. Lett. **92**, 201102 (2008).
[25]K. W. C. Chan, M. N. O'Sullivan, and R. W. Boyd, Opt. Lett. **34**, 3343-3345 (2009).
[26]Q. Liu, X. H. Chen, K. H. Luo, W. Wu, and L. A. Wu, Phys. Rev. A **79**, 053844 (2009).
[27]J. H. Shapiro, Phys. Rev. A **78**, 061802(R) (2008).
[28]O. Katz, Y. Bromberg, and Y. Silberberg, Appl. Phys. Lett. **95**, 131110 (2009).
[29]F. Ferri, D. Magatti, L. A. Lugiato, and A. Gatti, Phys. Rev. Lett. **104**, 253603 (2010).
[30]B. Sun, S. S. Welsh, M. P. Edgar, J. H. Shapiro, and M. J. Padgett, Opt. Exp. **20**, 16892-16901 (2012).
[31]B. Jack, J. Leach, J. Romero, S. Franke-Arnold, M. Ritsch-Marte, S. M. Barnett, and M. J. Padgett, Phys. Rev. Lett. **103**, 083602 (2009).
[32]N. Radwell, K. J. Mitchell, G. M. Gibson, M. P. Edgar, R. Bowman, and M. J. Padgett, Optica, **1**, 285-289 (2014).
[33]J. Shin, B. T. Bosworth, and M. A. Foster, Opt. Lett. **41**, 886-889 (2016).
[34]M. P. Edgar, G. M. Gibson, R. W. Bowman, B. Sun, N. Radwell, K. J. Mitchell, S. S. Welsh, and M. J. Padgett, Sci. Rep. **5**, 10669 (2015).
[35]H. Peng, Z. Yang, D. Li, and L. A. Wu. Proc. of SPIE **9795**, 97952O-1 (2015).
[36]N. Tian, Q. Guo, A. Wang, D. Xu, and L. Fu, Opt. Lett. **36**, 3302-3304 (2011).
[37]H. Yu, R. Lu, S. Han, H. Xie, G. Du, T. Xiao, and D. Zhu, Phys. Rev. Lett. **117**, 113901 (2016).
[38]D. Pelliccia, A. Rack, M. Scheel, V. Cantelli, and D. M. Paganin, Phys. Rev. Lett. **117**, 113902 (2016).
[39]R. I. Khakimov, B. M. Henson, D. K. Shin, S. S. Hodgman, R. G. Dall, K. G. H. Baldwin, and A. G. Truscott, Nature, **540**, 100-103 (2016).
[40]S. Gan, D. Z. Cao, and K. Wang, Phys. Rev. A, **80**, 043809 (2009).
[41]H. -C. Liu, Phys. Rev. A, **94**, 023827 (2016).
[42]L. -G. Wang, S. Qamar, S. -Y. Zhu, and M. S. Zubairy, Phys. Rev. A, **79**, 033835 (2009).